01 November 2023 13:13:13

RESEARCH ARTICLE | NOVEMBER 01 2023

# H₂O–HCN complex: A new potential energy surface and intermolecular rovibrational states from rigorous quantum calculations *⊗*

Patricia Vindel-Zandbergen ⑩ ; Dariusz Kędziera ⑩ ; Michał Żółtowski ⑩ ; Jacek Kłos ⑩ ; Piotr Żuchowski ⑩ ; Peter M. Felker ⑪ ; François Lique ⑪ ; Zlatko Bačić ➡ ⑩



J. Chem. Phys. 159, 174302 (2023) https://doi.org/10.1063/5.0173751





CrossMark

# H<sub>2</sub>O-HCN complex: A new potential energy surface and intermolecular rovibrational states from rigorous quantum calculations

Cite as: J. Chem. Phys. 159, 174302 (2023); doi: 10.1063/5.0173751 Submitted: 24 August 2023 • Accepted: 13 October 2023 •

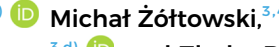






**Published Online: 1 November 2023** 

Patricia Vindel-Zandbergen, 1.a) Dariusz Kędziera, 2.b) Dariusz Kędziera, 2.b) Michał Żółtowski, 3.4 D Jacek Kłos, 5 D















# **AFFILIATIONS**

- Department of Chemistry, New York University, New York, New York 10003, USA
- <sup>2</sup> Faculty of Chemistry, Nicolaus Copernicus University in Toruń, ul. Gagarina 7, 87-100 Toruń, Poland
- <sup>3</sup>University of Rennes, CNRS, IPR (Institut de Physique de Rennes) UMR 6251, F-35000 Rennes, France
- LOMC UMR 6294, CNRS-Université du Havre, 25 rue Philippe Lebon, BP1123, 76 063 Le Havre cedex, France
- <sup>5</sup>Joint Quantum Institute, University of Maryland, College Park, Maryland 20742, USA
- <sup>6</sup>Institute of Physics, Faculty of Physics, Astronomy and Informatics, Nicolaus Copernicus University, ul. Grudziądzka 5, 87-100 Toruń, Poland
- Department of Chemistry and Biochemistry, University of California, Los Angeles, California 90095-1569, USA
- Simons Center for Computational Physical Chemistry at New York University, New York, New York 10003, USA
- 9NYU-ECNU Center for Computational Chemistry at NYU Shanghai, 3663 Zhongshan Road North, Shanghai 200062, China
- a) Electronic mail: patricia.vindel@nyu.edu
- b) Electronic mail: teodar@chem.umk.pl
- c) Electronic mail: felker@chem.ucla.edu
- d) Electronic mail: francois.lique@univ-rennes.fr
- e) Author to whom correspondence should be addressed: zlatko.bacic@nyu.edu

## **ABSTRACT**

In this work the H<sub>2</sub>O-HCN complex is quantitatively characterized in two ways. First, we report a new rigid-monomer 5D intermolecular potential energy surface (PES) for this complex, calculated using the symmetry-adapted perturbation theory based on density functional theory method. The PES is based on 2833 ab initio points computed employing the aug-cc-pVQZ basis set, utilizing the autoPES code, which provides a site-site analytical fit with the long-range region given by perturbation theory. Next, we present the results of the quantum 5D calculations of the fully coupled intermolecular rovibrational states of the H<sub>2</sub>O-HCN complex for the total angular momentum J values of 0, 1, and 2, performed on the new PES. These calculations rely on the quantum bound-state methodology developed by us recently and applied to a variety of noncovalently bound binary molecular complexes. The vibrationally averaged ground-state geometry of H<sub>2</sub>O-HCN determined from the quantum 5D calculations agrees very well with that from the microwave spectroscopic measurements. In addition, the computed ground-state rotational transition frequencies, as well as the B and C rotational constants calculated for the ground state of the complex, are in excellent agreement with the experimental values. The assignment of the calculated intermolecular vibrational states of the H<sub>2</sub>O-HCN complex is surprisingly challenging. It turns out that only the excitations of the intermolecular stretch mode can be assigned with confidence. The coupling among the angular degrees of freedom (DOFs) of the complex is unusually strong, and as a result most of the excited intermolecular states are unassigned. On the other hand, the coupling of the radial, intermolecular stretch mode and the angular DOFs is weak, allowing straightforward assignment of the excitation of the former.

Published under an exclusive license by AIP Publishing. https://doi.org/10.1063/5.0173751

#### I. INTRODUCTION

Noncovalent, hydrogen-bonded and van der Waals (vdW) interactions are ubiquitous in nature and of profound importance, as they have a major role in governing the structural and dynamical properties of matter ranging in size from small molecular complexes and molecular clusters to solid and liquid condensed phases, as well as macromolecules of biological importance and their supramolecular complexes. This has made noncovalent interactions the focus of intense research by experimentalists and theorists alike for decades, and the attention they receive continues unabated. Noncovalently bound molecular complexes, dimers in particular, represent uniquely attractive targets that allow the study of the intricate rovibrational dynamics dominated by nuclear quantum effects on potential surfaces with multiple minima, at the level of detail and accuracy that would be impossible for more complex systems. These investigations have been characterized by a fruitful interplay between advanced high-resolution spectroscopic techniques, ab initio electronic structure calculations, and high-level multidimensional quantum calculations of the rovibrational eigenstates and

Accurate description of the interactions of water with other molecules is of great fundamental and practical significance for achieving quantitative understanding of many aspects of Earth's atmospheric chemistry, processes in comets, protoplanetary disks, and the interstellar medium. This has motivated detailed spectroscopic and theoretical studies of numerous binary watercontaining complexes. A number of them have been the subject of sophisticated fully coupled quantum calculations of their rovibrational states. Some of these calculations were performed using a rigid-monomer approach, e.g., for H<sub>2</sub>O/D<sub>2</sub>O-CO<sub>2</sub>, H<sub>2</sub>O-HF,  $H_2O-H_2$ , and CH<sub>4</sub>-H<sub>2</sub>O.<sup>9,10</sup> Owing to recent methodological advances, 11,12 it has also become possible to perform full-dimensional and fully coupled quantum computations of the (ro)vibrational states of water-containing binary molecular complexes for flexible monomers, H<sub>2</sub>O/D<sub>2</sub>O-CO, <sup>13</sup> HDO-CO, <sup>14</sup> H<sub>2</sub>O-HCl,<sup>15</sup> and several of its H/D isotopologues, <sup>16,17</sup> benzene-H<sub>2</sub>O/HDO (flexible water and rigid benzene), <sup>18</sup> and most recently

HCN, a well-known hydrogen-bond forming molecule, is one of the most observed molecules in the interstellar medium (ISM) and is considered as excellent tracer of high-density regions due its relatively large dipole moment. The formation path of HCN in comets is not well known. HCN could be sourced either from the inheritance of HCN ice formed early in the star formation sequence, or through active synthesis during the protoplanetary disk stage. Accurate determination of its abundance (which can help in constraining its formation process) can only be obtained through advanced nonlocal-thermal-equilibrium (non-LTE) models,<sup>2</sup> which require radiative and collisional properties of the molecule. Interaction between HCN and H<sub>2</sub>O (the dominant collider in cometary comae) is then of high interest.

Initially, the H<sub>2</sub>O-HCN complex was investigated by *ab initio* calculations at the Hartree-Fock level<sup>22</sup> and more accurate theoretical studies were performed subsequently. 23-26 Recently, a 5D potential energy surface (PES) for the water-HCN system was calculated ab initio at the coupled-cluster CCSD(T) level of theory, treating both monomers as rigid, and a global fit was introduced to describe the water-HCN interaction.<sup>27</sup> This PES reproduces the two isomers reported previously in the literature, <sup>25,26,28</sup> in which H<sub>2</sub>O and HCN can act as both proton donors and acceptors, and predicts rotational constants in good agreement with previous experimental and theoretical studies. In the follow-up work,<sup>29</sup> the authors employed this PES to investigate the rotational excitation of HCN by water using the coupled-states scattering approach and provide approximate rotational de-excitation rate coefficients among the first levels of HCN perturbed by para-water in the temperature range T = 5-150 K. The H<sub>2</sub>O-HCN complex has also been the subject of several microwave spectroscopic studies, 30-32 which have provided information regarding its ground-state geometry, rotational constants, rotational transition frequencies, and other

In this paper we report a new rigid-monomer 5D intermolecular PES of the H<sub>2</sub>O-HCN complex, computed using the symmetry-adapted perturbation theory based on density functional theory [SAPT(DFT)] method  $^{33}$  and the autoPES code.  $^{34,35}$  The level of accuracy of this approach is comparable to that of CCSD(T), but with the numerical cost reduced by two orders of magnitude. The second objective of this paper is to utilize the new PES in the quantum 5D calculations of the fully coupled intermolecular vibrational states of the H<sub>2</sub>O-HCN complex in the rigid-monomer approximation for the total angular momentum J values of 0, 1, and 2. Keeping the monomers rigid decreases the dimensionality of the problem from 12D to 5D, making the calculations far more manageable. The errors in the bound-state calculations introduced by the assumption of rigid monomers are expected to be small due to the weak coupling between the intermolecular vibrations of the complex and the intramolecular vibrations of the monomers in their ground states. In the case of the similar complex H<sub>2</sub>O-HCl,<sup>15</sup> the energies of the intermolecular vibrational levels from full-dimensional (9D) and rigid-monomer (5D) calculations typically differ by  $1-3 \text{ cm}^{-1}$ .

These calculations employ the methodology used previously in the quantum 5D rigid-monomer calculations of the rovibrational states of the H<sub>2</sub>O-CO<sub>2</sub> and D<sub>2</sub>O-CO<sub>2</sub> vdW complexes.<sup>1</sup> In addition to the rovibrational states of H<sub>2</sub>O-HCN, the calculations yield the vibrationally averaged ground-state geometry of the complex, its rotational constants and rotational transition frequencies in the ground vibrational state. Comparison is made with the spectroscopic data in the literature, and very good agreement is found between theory and experiment.

The paper is organized as follows. Section II presents the ab initio methodology and the calculations involved in the development of the 5D PES of the H<sub>2</sub>O-HCN complex and describes its key features. The methodology employed in the quantum 5D calculations of the intermolecular rovibrational states of the complex on this PES is described in Sec. III. In Sec. IV, we present and discuss the results of these calculations. Conclusions are given in Sec. V.

# II. H<sub>2</sub>O-HCN POTENTIAL ENERGY SURFACE A. SAPT(DFT)/AUTOPES calculations

The H<sub>2</sub>O-HCN potential energy surface was calculated with the symmetry-adapted perturbation theory based on density functional theory [SAPT(DFT)]33,36-38 and the aug-cc-pVQZ atomic basis set. The interaction potential between H<sub>2</sub>O and HCN molecules in their respective electronic ground states was generated using the autoPES code. 34,35 One of the key advantages of this code is the use of multipolar expansion for an accurate description of the long-range region, which can then be seamlessly connected to the valence-overlap region. Such approach reduces the number of sampled geometries required for obtaining the PES by one or even two orders of magnitude, as one has only to take care of the short-range region and the vicinity of minima. In addition, autoPES is compatible with fast and reliable methods like density fitting techniques, notably DF-SAPT(DFT). It was recently demonstrated that the accuracy of SAPT(DFT) approaches is similar to that of CCSD(T) but with a numerical cost reduced by two orders of magnitude ( $N^5$  compared to  $N^7$ , with N the number of electrons).<sup>39</sup> Our calculations used DF-SAPT(DFT) based on the asymptotically corrected PBE0 functional.40 The aug-cc-pVQZ basis set41-43 was employed for all atoms.

As a default setting, midbond functions with the M1 basis set, taken from the SAPT library, were included in the basis set for every geometry for which the interaction energy was computed.

The SAPT(DFT) calculations require a gradient-regulated asymptotic correction (GRAC)<sup>44</sup> of exchange-correlation functionals. The parameters needed for such a procedure are ionization energies. The values used in our SAPT(DFT) calculations are 12.6308 eV for H<sub>2</sub>O and 13.5531 eV for HCN. We included a  $\delta_{HF}$  term in our calculations, which takes into account higher-order induction.

AutoPES constructs a site-site potential with electrostatic, polarization, induction-plus-dispersion, and repulsive exponential components of energy that can be enabled. Thus, the number of fitting potential parameters depends on the number of sites. In addition to the sites located on the atoms, off-atomic sites, i.e., points that are not located on the atoms, were are added to enhance the flexibility of the fitting function. The root-mean-square error (RMSE) of the fitted PES within the attractive region with sites on the atoms of the complex was about 130 cm $^{-1}$  for H2O–HCN. By adding nine off-atomic sites to the H2O molecule and four to HCN, the RMSE was decreased to 7 cm $^{-1}$  for the attractive region.

We treat  $\rm H_2O$  and HCN molecules as rigid monomers. The geometry of the  $\rm H_2O$  species was fixed with  $r_g(\rm OH)=1.8437~a_0$  and the bond angle of  $104.4^{\circ}$ . Vibrationally averaged bond lengths  $r_g(\rm CH)$  and  $r_g(\rm CN)$  for linear HCN were calculated according to formula:  $^{46}$ 

$$r_{g}(i) = r_{e}(i) + \langle \Delta r(i) \rangle, \tag{1}$$

where  $r_e(i)$  is the equilibrium bond length, and the displacement  $\langle \Delta r(i) \rangle$  is the correction of a given bond length due to averaging over vibrations. The  $r_e(i)$  values were obtained by complete basis set (CBS) extrapolation of non-relativistic bond distances calculated with CCSD(T) method with aug-cc-pCVXZ basis sets for X=Q,5,6 and then improved by including a relativistic correction to the bond length calculated within X2C-CCSD(T) method. Throducing the relativistic corrections results in a slight reduction of bond lengths, by 0.003  $a_0$  for the CH bond and by 0.004  $a_0$  for the CN bond. Obtained  $r_e(CH)=2.0126$   $a_0$  and  $r_e(CN)=2.1777$   $a_0$  are negligibly smaller than the values derived from the experiment by Gisbert *et al.*, 48 2.0135  $a_0$  and 2.1792  $a_0$ , respectively. Displacements  $\langle \Delta r(i) \rangle$  were obtained from a cubic force field expansion of the PES

calculated within CCSD(T). They were extrapolated to CBS from ccpCVXZ values for X = T, Q, 5 leading to  $\langle \Delta r(CH) \rangle = 0.0336 \ a_0$  and  $\langle \Delta r(CN) \rangle = 0.0097 \ a_0$ . Finally, we obtained  $r_g(CH) = 2.0462 \ a_0$  and  $r_g(CN) = 2.1874 \ a_0$ .

Geometry optimization and averaging for all monomers were performed with the help of the CFOUR quantum chemistry package.  $^{49,50}$ 

#### B. Analysis and contour plots

To describe the dimer interaction and to calculate the H<sub>2</sub>O-HCN PES, we follow the convention of Phillips et al.,<sup>51</sup> where the water (monomer A) orientation is fixed in the  $(x_A, y_A, z_A)$  Cartesian system of coordinates by coupling the body-fixed (BF) frame to the water molecule in such a way that its origin  $(x_A, y_A, z_A)$ = (0,0,0) is at the centre of mass, its  $z_A$  axis is along the  $C_2$  symmetry axis, and its  $x_A z_A$  plane is the plane of the water molecule as shown in Fig. 1. The HCN molecule (monomer B) is described by the  $(x_B, y_B, z_B)$  system of coordinates with its origin  $(x_B, y_B, z_B)$ = (0,0,0) in its center of mass. The corresponding axes of both of these Cartesian system of coordinates are parallel. In panel (a) of Fig. 1 we show Brocks-type of internal coordinates used in the bound state calculations and panel (b) shows the polar coordinates that we use for the determination of the five-dimensional  $V(R, \theta, \phi, \theta', \phi')$  PES. R is the vector between the centers of mass (c.m.) of the monomers and  $(\theta, \phi)$  and  $(\theta', \phi')$  define the polar angles that describe the orientation of R and HCN, respectively, as illustrated in panel (b) of Fig. 1.

To determine the entire five-dimensional H<sub>2</sub>O-HCN PES we needed just a total of 2833 *ab initio* points for which two minima

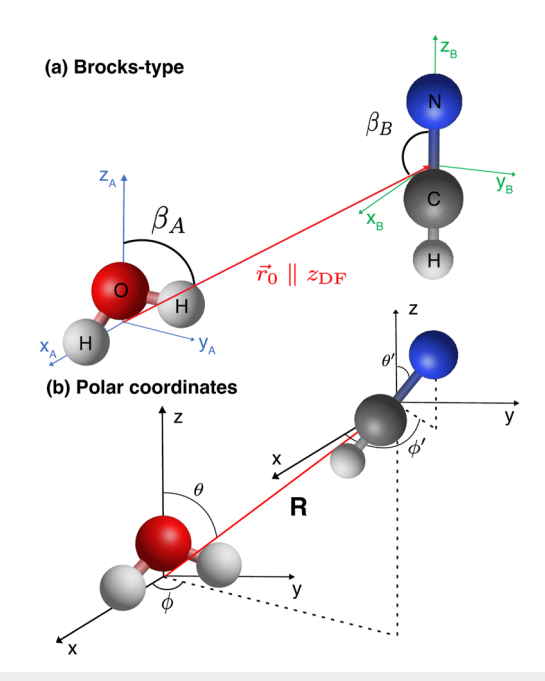


**FIG. 1.** 5D body-fixed coordinate systems used to describe  $H_2O$ –HCN interaction. (a) Brock-type approach. (b) The orientation of the c.m. to c.m R vector and the orientation of the HCN molecule are both described with respect to the water-fixed axes by the polar angles  $(\theta, \phi)$  and  $(\theta', \phi')$ , respectively. See Refs. 27 and 51.

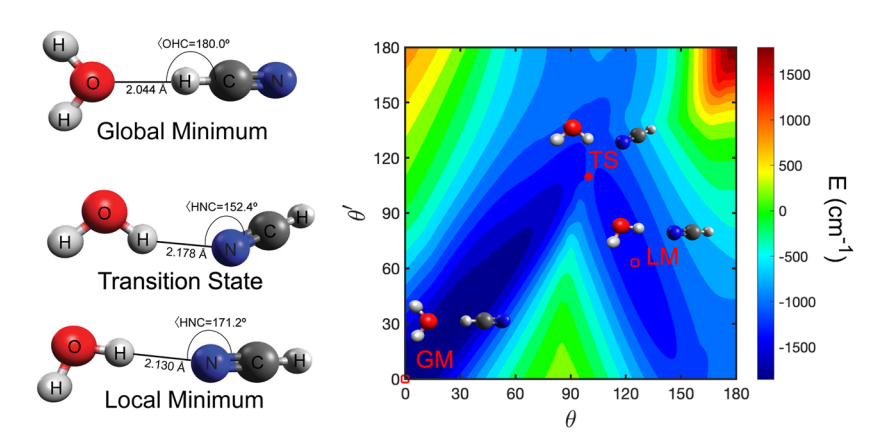


**FIG. 2.** Contour plot of the H<sub>2</sub>O-HCN PES as a function of  $\theta$  and  $\theta'$  coordinates (in deg) [minimized over  $(R, \phi, \phi')$  coordinates]. The transition state (TS) indicated by red star symbol represents a barrier between the global (GM) and local (LM) minima (locations represented by red squares). The energy of the transition state is  $E_{TS} = -1190.5 \text{ cm}^{-1}$ .

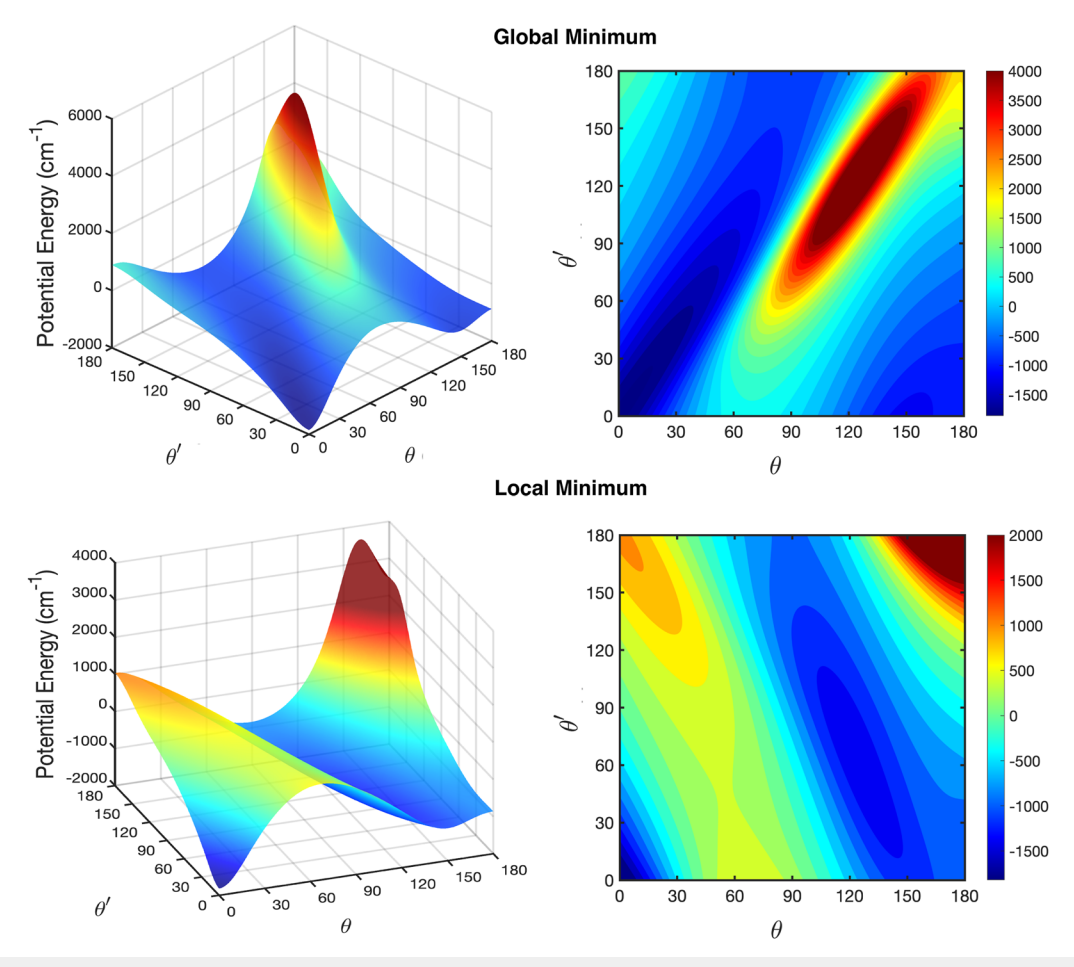


**FIG. 3.** Top left: Surface plot of the  $(\theta, \theta')$  angular cut in the region of the global minimum at R = 3.753 Å for  $\phi = \phi' = 0^{\circ}$ . Top right: contour plot of the same global minimum region. Bottom left: Surface plot of the  $(\theta, \theta')$  angular cut in the region of the local minimum at R = 3.658 Å for  $\phi = \phi' = 0^{\circ}$ . Bottom panel: contour plot of the same local minimum region. All angles are given in degrees and energies in units of cm<sup>-1</sup>.

were found, that are separated by a barrier of 661.84 cm<sup>-1</sup> as shown in Fig. 2. The barrier was calculated by subtracting the energy of the saddle point (-1190.5 cm<sup>-1</sup>, at  $\theta = 100$ ,  $\phi = 0$  and  $\theta' = 110$ ,  $\phi' = 180'$ , see Fig. 2) from the energy of global minimum (-1852.35 cm<sup>-1</sup>). The global minimum (Fig. 2) was found for a configuration where the hydrogen of HCN approaches the oxygen of the water molecule (HCN acts as the proton donor). The energy for the global minimum was found to be -1852.35 cm<sup>-1</sup> while the distance between the hydrogen of HCN and oxygen atom of water is 2.044 Å. Comparing this result with the global minimum reported by Dubernet and Quintas-Sánchez et al.,27 which has an energy of -1814.51 cm<sup>-1</sup>, we find that the potential well calculated in this work is slightly deeper. We show the region of the global minimum as a function of the  $\theta$  and  $\theta'$  polar angles in Fig. 3. The local minimum shown in Fig. 2, with the energy of -1338.36 cm<sup>-1</sup>, is located at a geometry where the nitrogen atom is approaching one of the hydrogens of the water molecule. The distance between these atoms was found to be 2.130 Å. Comparing this to the local minimum reported by Dubernet and Quintas-Sánchez et al.,27 who reported the energy of -1377.30 cm<sup>-1</sup>, the interaction energy that we determined is in this case slightly less attractive. Figure 3 shows the surface and contour plots of the PES in the region of the global and local minima of the dimer. Such a difference between the two minima of these two PESs may be accounted for by the different *ab initio* method used in calculations - SAPT(DFT) in this work and CCSD(T) in Dubernet and Quintas-Sánchez *et al.*,<sup>27</sup> as well as the basis set size used in the calculations.

To assess the accuracy of the  $H_2O$ –HCN PES, additional *ab initio* calculations were performed for characteristic geometries (the global and local minima) and several distances between the centers of mass of the two monomers. We used the CCSD(T) method implemented in the MOLPRO code<sup>52</sup> with aug-cc-pCVXZ basis sets for X = D, T, Q. Three different basis sets were used in the calculations to perform extrapolations to the CBS limit, using a mixed Gaussian/exponential extrapolation scheme.<sup>53</sup>

Results from these calculations are presented in Fig. 4. For the global minimum of  $H_2O$ –HCN, the result obtained with the SAPT(DFT) method ( $-1852.35~{\rm cm}^{-1}$ ) slightly overestimates, by 2.65 cm<sup>-1</sup>, the result obtained with the CBS extrapolation ( $-1849.7~{\rm cm}^{-1}$ ). On the other hand, for the local minimum, the well

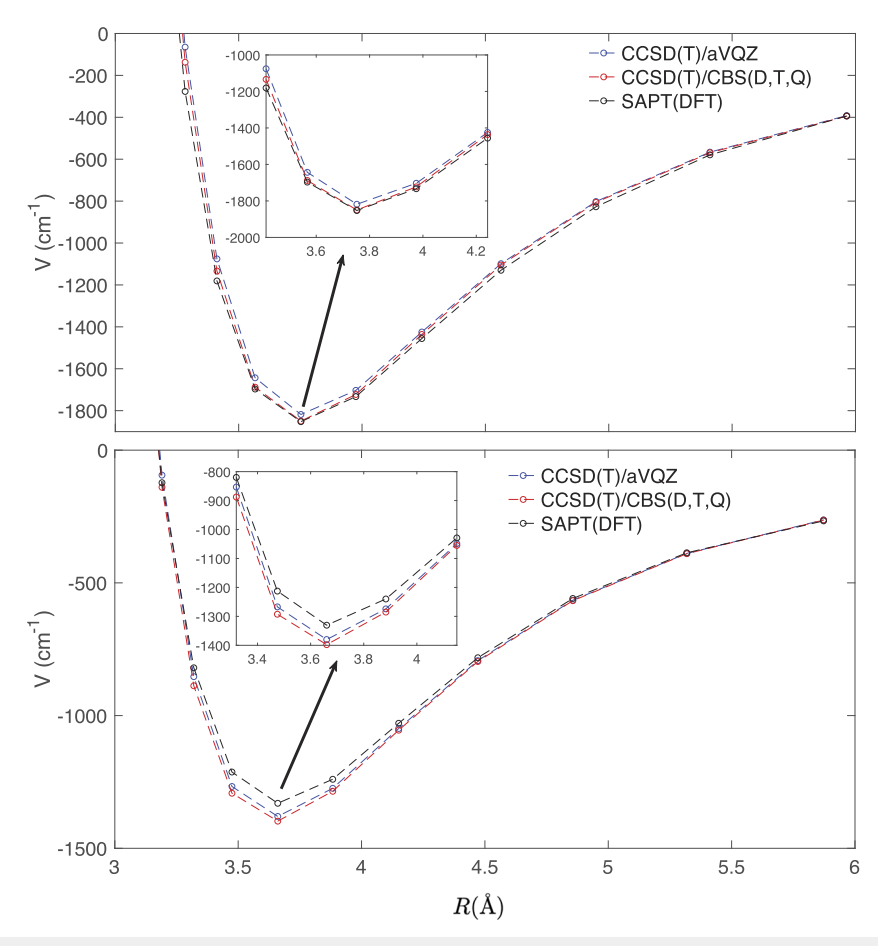


FIG. 4. Comparison of interaction energy at different levels of theory as a function of distance between the center of mass of the monomers for the geometries of global (upper panel) and local (lower panel) minimum of H<sub>2</sub>O–HCN system. See the text for details.

obtained with the SAPT(DFT) method (-1338.36 cm<sup>-1</sup>) is shallower by 59.7 cm<sup> $^{-1}$ </sup> than the one based on CCSD(T)/CBS ( $-1397.70 \text{ cm}^{-1}$ ) The difference with respect to CCSD(T) is somewhat significant and might result from several factors: differences between the description of the intramonomer dynamics correlation between PBE0 and CCSD(T), as well as lack of electronic correlation beyond the second order of SAPT ( $\delta_{\rm HF}$  is based on supermolecular Hartree-Fock calculations). The overall agreement is good and a PES of such accuracy can be safely used for bound states or scattering calculations. It is noteworthy that neglecting the  $\delta_{HF}$  term leads to inaccuracies on the order of more than 10% near both the global and local minima. Therefore, it is crucial to include this term when calculating the PESs for polar systems. This observation aligns with previously reported behavior of SAPT for water-bearing complexes.3

The computer code for generating this H<sub>2</sub>O-HCN PES is provided in the supplementary material.

#### III. COMPUTATIONAL METHODOLOGY FOR ROVIBRATIONAL STATES

#### A. General

The computational results presented relate to the intermolecular rovibrational states of H<sub>2</sub>O-HCN molecular complexes in the rigid-monomer approximation. We follow the same procedure presented in Ref. 1. We employ the "Brocks-type" approach introduced in Ref. 54, the Hamiltonian and associated coordinates are adapted to the water-HCN complexes. In this method, the dimer-fixed coordinate frame is defined in terms of the vector pointing from the c.m. of one monomer to that of the other, as illustrated in Fig. 1.

We require as input the rigid-monomer geometries and inertial parameters, given in Sec. II A. We use the following: for HCN, we take the rotational constant as B = 1.4782218 cm<sup>-148</sup> and the mass to be 27.0257 amu. For the rotational constants of H<sub>2</sub>O we use  $B_{x_A} = 27.8761 \text{ cm}^{-1}$ ,  $B_{y_A} = 9.2877 \text{ cm}^{-1}$  and  $B_{z_A} = 14.5074 \text{ cm}^{-1}$ , where  $x_A$ ,  $y_A$  and  $z_A$  refer to the principal axes of the H<sub>2</sub>O moiety (see Sec. II B). The H<sub>2</sub>O mass is 18.0103 amu.

The PES describing the H<sub>2</sub>O-HCN interaction was adapted from the coordinate system described in Sec. II B to the Brockstype coordinate system, that is, we convert the polar coordinates  $(R, \theta, \phi, \theta', \phi')$  to the coordinates used in the Brocks-type approach. Another minor modification was required: we found evidence for an unphysical "hole" in regions corresponding to small intermonomer distances, then we set the interaction PES to a large value (0.01 hartree) for all dimer geometries at which one (or all) of the O(H<sub>2</sub>O) and H(H<sub>2</sub>O) to H(HCN), C(HCN) and N(HCN) internuclear distances is smaller than 1.375 Å. We do not expect significant wavefunction amplitude in the regions below our distance thresholds, since at short atom-atom distances the PES should be large. Therefore any possible discontinuities introduced in the PES by our fix should have no effect on our results. This fix is justifiable physically and eliminates any influence of the "hole" on our results.

#### B. The Brocks-type approach

#### 1. Coordinates and Hamiltonian

As specified in Brocks et al.,54 we define a dimer-fixed (DF) frame for the dimer with its origin at the c.m. of the dimer. The DF-frame axes are rotated by the Euler angles  $\Omega = (\alpha, \beta)$  from a

space-fixed (SF) frame, and its z axis  $(\hat{z}_{DF})$  is parallel to the vector  $\mathbf{r}_0$ that points from the c.m. of monomer A (H2O) to that of monomer B (HCN). Next, we define the monomer-fixed frame for monomer A (MFA) as the principal axis frame of the H2O moiety, with 2A along the  $C_2$  symmetry axis pointing toward the O nucleus,  $\hat{v}_A$  as the out-of-plane principal axis parallel to the vector defined by the cross product of the O-to-H1 bond vector and the O-to-H2 bond vector, and  $\hat{x}_A = \hat{y}_A \times \hat{z}_A$ . The z axis fixed to HCN  $(\hat{z}_B)$  is the unit vector pointing from the C atom of that moiety to the N atom. Finally, we define the following coordinates: (i)  $r_0 \equiv |\hat{\mathbf{r}}_0|$ , (ii)  $\omega_A \equiv (\alpha_A, \beta_A, \gamma_A)$ , the Euler angles that define the orientation of BFA with respect to DF, and (iii)  $\omega_B \equiv (\alpha_B, \beta_B)$ , the Euler angles that define the orientation of  $\hat{z}_B$  with respect to DF (see Fig. 1). The third Euler angle,  $\gamma_B$ , is not needed as HCN is a linear molecule. We can express now the intermolecular Hamiltonian as:

$$\hat{H}_{inter}(\mathbf{Q}, \Omega) = \hat{T}_{inter}(\mathbf{Q}, \Omega) + \hat{T}_{rot}^{A}(\omega_{A}) + \hat{T}_{rot}^{B}(\omega_{B}) + V_{inter}(\tilde{\mathbf{Q}}),$$
(2)

where  $\mathbf{Q} \equiv (r_0, \omega_A, \omega_B)$  and  $\tilde{\mathbf{Q}} \equiv (r_0, \tilde{\alpha}, \beta_A, \gamma_A, \beta_B)$ . Note that the dimer potential is independent of the individual values of  $\alpha_A$  and  $\alpha_B$  and is dependent only on their difference,  $\tilde{\alpha} \equiv (\alpha_A - \alpha_B)$ . The intermolecular kinetic energy operator,  $\hat{T}_{inter}$  is that from Brocks

$$\hat{T}_{inter} \equiv -\frac{1}{\mu_D} \frac{\partial^2}{\partial r_0^2} + \frac{1}{2\mu_D r_0^2} \times \left[ \mathbf{J}^2 - \cot \beta \frac{\partial}{\partial \beta} + (\mathbf{j}^A + \mathbf{j}^B)^2 - 2\mathbf{J} \cdot (\mathbf{j}^A + \mathbf{j}^B) \right], \quad (3)$$

where  $\mu_D$  is the reduced mass of the dimer, **J** is the is the vector operator corresponding to the rotational angular momentum of the dimer measured with respect to the DF frame, and  $j^{A}$  and  $j^{B}$  are the vector operators corresponding, respectively, to the rotational angular momenta of the H<sub>2</sub>O and HCN moieties measured with respect to the DF frame.  $\hat{T}_{rot}^A(\omega_A)$ , the rigid-rotor rotational kinetic-energy operator of the H<sub>2</sub>O monomer, is given by

$$\hat{T}_{rot}^{A}(\omega_{A}) \equiv \sum_{i_{A}} B_{i_{A}} (\hat{j}_{i_{A}}^{A})^{2}$$
(4)

where  $i_A$  is an index that runs over the principal axes of H<sub>2</sub>O and  $\hat{j}_{i_A}^A$ is the operator associated with the rotational angular momentum of the  $H_2O$  moiety along axis  $i_A$ . Similarly,

$$\hat{T}_{rot}^B(\omega_B) \equiv B(\hat{j}^B)^2 \tag{5}$$

is the rigid-rotor rotational kinetic-energy operator of the HCN monomer. Finally,  $V_{inter}(\tilde{\mathbf{Q}})$  is the 5D intermolecular potential function described in Sec. II. The integration volume element associated with this  $\hat{H}_{inter}$  is of the Wilson type:<sup>55</sup>  $dr_0 d\omega_A d\omega_B d\Omega$ . This choice facilitates the construction of the potential-optimized discrete variable representation (PODVR) covering the  $r_0$  coordinate (see Sec. III B 2).

#### 2. Basis sets

In order to solve for the eigenstates of  $\hat{H}_{inter}$ , we use "uncoupled" basis functions of the Brock type. These are of the form

$$|s, j_A, k_A, m, j_B; J, K\rangle \equiv |r_{0,s}\rangle |j_A, k_A, m\rangle |j_B, K - m\rangle |J, K\rangle,$$
 (6)

where the  $|r_{0,s}\rangle$   $(s = 1, ..., N_{r_0})$  are potential-optimized DVR  $(PODVR)^{56,57}$  functions covering the  $r_0$  degree of freedom, the  $|j_A, k_A, m\rangle$ ,  $j_A = 0, 1, \dots, j_A^{\text{max}}$ , are symmetric-top eigenfunctions dependent on the  $\omega_A$  coordinates, and the  $|j_B, -m\rangle$ ,  $(j_B = 0, 1, \dots, j_B^{\text{max}})$  are spherical harmonics dependent on the  $\omega_B$ coordinates, and the  $|J,K\rangle$  are normalized "little-d" Wigner matrix elements of the form

$$|J,K\rangle \equiv \sqrt{\frac{2J+1}{2}}d_{0,K}^{J}(\beta). \tag{7}$$

The full basis for a given value of J ( $\hat{H}_{inter}$  is block-diagonal in J) consists of all those functions of the type in Eq. (6) whose  $k_A$  and mvalues are allowed, given the values of  $j_A$  and  $j_B$ .

H<sub>2</sub>O-HCN belongs to the molecular symmetry group  $G_4 = [E, (12), E^*, (12)^*]$ , where (12) is the water-hydrogen-nucleus interchange operator and  $E^*$  is the inversion operator. These symmetry operators leave  $\hat{H}_{inter}$  invariant. Thus, the intermolecular Hamiltonian can be block diagonalized into four blocks corresponding to the four irreducible representations ("irreps") of  $G_4$ . The reader is referred to Sec. II 3 C of Ref. 13 for details.

In this work the basis parameters are as follows: (1)  $N_{r_0} = 50$ with the  $|r_{0,s}\rangle$ ,  $(s=1,\ldots,N_{r_0})$  DVR points ranging from 2.3 to 8.31 Å, (2)  $j_{\max}^A = 12$ , and (3)  $j_{\max}^B = 30$ . We settled on these basisset parameters after varying each of them over a range of values and performing convergence tests. For these parameters and J = 0, the numbers of basis states, absent any symmetry sorting, are 1 919 950. The corresponding numbers for J = 1 are 5 703 600, and 9 557 450 for J = 2. The number of independent basis states corresponding to the symmetry-sorted blocks is about a factor of four smaller than those listed above.

The  $|r_{0,s}\rangle$ ,  $(s = 1, ..., N_{r_0})$  PODVR was constructed by first solving the 1D Schrödinger equation

$$-\frac{1}{2\mu_0}\frac{\partial^2 \psi}{\partial r_0^2} + V_{\text{eff}} = E_0 \psi \tag{8}$$

in a sinc-DVR grid of 150 functions ranging from 2.12 to 8.47 Å. The  $V_{\text{eff}}(r_0)$  in Eq. (8) is  $V_{inter}(\tilde{\mathbf{Q}})$  minimized with respect to all the coordinates except  $r_0$  at each one of the  $r_0$  sinc-DVR points. The 50 lowest-energy eigenfunctions from Eq. (8) were then used to construct the PODVR per Refs. 56 and 57.

## 3. Diagonalization of Ĥ<sub>inter</sub>

To diagonalize  $\hat{H}_{inter}$  we exploit the  $G_4$  invariance of that operator to solve separately for the eigenvalues and eigenvectors associated with the four  $G_4$  symmetry blocks. We obtain the eigenstates and energies for a given value of J and for specific values of  $E^*$ and (12) symmetry operators by Chebyshev filter diagonalization.<sup>58</sup> We apply successive operations of  $\hat{H}_{inter}$  on a symmetry-filtered, random initial state vector in two steps. First, we operate with the kinetic-energy portion of  $\hat{H}_{inter}$  by direct matrix-vector multiplication. Second, we operate on the state vector with the potentialenergy part of the Hamiltonian by (i) transformation of the state vector to a 5D  $(r_0, \cos \beta_A, \gamma_A, \cos \beta_B, \tilde{\alpha})$  quadrature-grid representation, (ii) multiplication of the state vector in that form by the value of the potential  $V_{inter}$  at each grid point, and (iii) transformation of the result back to the  $|s, j_A, k_A, m, j_B\rangle$  basis representation. The procedure is detailed in Sec. II B 3 of Ref. 1 and Sec. II C 2 of Ref. 13.

#### 4. Rotational constants in the rigid-monomer approximation

We calculated the principal rotational constants of the H<sub>2</sub>O-HCN complex for a given vibrational state from the 5D results by subtracting the J = 0  $\hat{H}_{inter}$  eigenvalue corresponding to that vibrational state from each of the three J = 1 eigenvalues for that state to obtain the three rotational energies, in increasing order:  $E_{01}$ ,  $E_{11}$ , and  $E_{10}$ . We then used the following rigid-rotor relations to compute the rotational constants:

$$A = \frac{E_{10} + E_{11} - E_{01}}{2}$$

$$B = \frac{E_{10} + E_{01} - E_{11}}{2}$$

$$C = \frac{E_{11} + E_{01} - E_{10}}{2}.$$
(9)

For accurate values of A, B, and C, it is essential that the J = 0 and J = 1 calculations have the same degree of convergence. In addition, one can compute the rotational constants from J = 2calculations, using the analytical expressions for their energies.<sup>55</sup>

#### IV. RESULTS AND DISCUSSION

#### A. Vibrationally averaged ground-state geometry

Low-energy J = 0 intermolecular vibrational states of the H<sub>2</sub>O-HCN complex are presented in Table I. The level energies are measured from their quantum 5D ground-state energy at -1488.342 cm<sup>-1</sup> relative to the separated rigid monomers. As described already in Sec. II B, the PES of the complex has two minima corresponding to the isomers shown in Fig. 2, the global minimum where the H<sub>2</sub>O molecule acts as the proton acceptor and HCN as the proton donor, and the local minimum that is 513.99 cm<sup>-1</sup> above the global minimum, in which the roles of the two monomers are reversed. The 5D zero-point energy (ZPE) of the  $H_2O$ -HCN complex is 364.64 cm<sup>-1</sup>.

In the global minimum, the equilibrium geometry is planar, with  $C_{2v}$  symmetry. However, the monomers in the complex can execute large-amplitude intermolecular motions. The geometries at the local minimum and at the barrier are of lower symmetry, with a single plane of symmetry and hence, they belong to the Cs point-group. This raises the question of the effective, vibrationally averaged ground-state geometry of the H<sub>2</sub>O-HCN complex, which has received considerable attention. 25-28,30-32 The coordinates most useful for characterizing the geometry of the complex, and for comparison with microwave spetroscopic studies,  $^{30,31}$  are  $\beta_A$ , the polar angle between the  $C_2$  axis  $H_2O$  and the vector  $\mathbf{r}_0$  connecting the c.m. of  $H_2O$  to that of the HCN (same as R in Sec. II B), and  $\beta_B$ , the polar angle between molecular axis of HCN and  $\mathbf{r}_0$ . For both  $\bar{\beta}_B = 0^{\circ}$  and  $\beta_B = 180^{\circ}$ , the three atoms of HCN lie on the inter-monomer axis. However, when  $\beta_B = 180^{\circ}$ , the H atom of HCN is the one closest to the c.m. of H<sub>2</sub>O, corresponding to the H<sub>2</sub>O···HCN isomer/global minimum. On the other hand, when  $\beta_B = 0^{\circ}$ , it is the N atom of HCN that is the closest to the c.m of the  $H_2O$  moiety, corresponding to the  $HCN \cdot \cdot \cdot H_2O$  isomer/local minimum.

Given in Table I for each intermolecular state are  $\langle \beta_A \rangle$  and  $\langle \beta_B \rangle$ , the expectation values of  $\beta_A$  and  $\beta_B$ , respectively, for that state. They are calculated as  $\langle \beta_i \rangle = \cos^{-1} \langle \cos \beta_i \rangle$ , where  $\langle \cos \beta_i \rangle$  is the expectation value of  $\beta_i$  for a given state and i = A, B. One can see that in the

**TABLE I.** Low-energy intermolecular vibrational states of H<sub>2</sub>O–HCN from the quantum 5D calculations (in cm<sup>-1</sup>).  $\langle r_0 \rangle$  and  $\Delta r_0$  (in Å),  $\langle \beta_A \rangle$ ,  $\Delta \beta_A$ ,  $\langle \beta_B \rangle$ ,  $\Delta \beta_B$  (in deg) are defined in the text. "Irrep." refers to the irreducible representations of  $G_4$ , for which g/u denote even/odd wavefunction parity and A/B denote symmetric/antisymmetric wavefunction transformation upon water–hydrogen nuclei exchange.

Irrep.	$E (cm^{-1})$	$\langle r_0  angle$	$\Delta r_0$	$\langle eta_A \rangle$	$\Deltaoldsymbol{eta}_A$	$\langle \beta_{\scriptscriptstyle B} \rangle$	$\Deltaoldsymbol{eta}_B$	Assign.
$\overline{\mathbf{A}_g}$	0	3.776	0.109	27.942	6.933	170.127	0.859	g.s.
$B_g$	94.631	3.757	0.110	31.299	7.277	166.114	1.318	_
$B_u$	112.514	3.768	0.110	34.981	9.740	166.58	1.261	
$A_g$	128.65	3.824	0.190	28.493	7.105	169.504	1.031	$v_{ m st}$
$A_g$	174.288	3.749	0.120	34.667	8.824	162.833	2.005	$ u_{\mathrm{b}}$
$B_u$	178.238	3.779	0.110	37.038	9.626	169.151	1.031	$v_{ m inv}$
$B_g$	217.665	3.791	0.191	32.494	7.678	164.673	1.719	
$A_u$	227.084	3.749	0.112	38.741	10.084	163.383	1.604	
$A_g$	232.162	3.755	0.113	39.864	11.287	163.457	1.604	
$B_u$	237.827	3.815	0.193	35.25	9.912	165.856	1.432	
$A_g$	251.131	3.877	0.248	28.98	7.334	169.003	1.146	$2v_{\rm st}$
$B_g$	256.959	3.756	0.130	34.606	8.308	162.191	2.636	
$\mathbf{B}_{g}$	263.109	3.779	0.122	32.409	8.136	165.933	1.891	
$A_u$	271.151	3.761	0.112	38.689	9.397	165.232	1.432	
$A_g$	285.097	3.769	0.116	39.235	12.605	165.148	1.719	
$B_u$	288.623	3.748	0.124	41.75	12.49	160.056	2.578	$v_{\rm inv} + v_{\rm b}$
$A_g$	290.145	3.770	0.124	36.213	9.454	160.812	2.636	
$B_u$	304.267	3.829	0.192	37.852	9.912	168.637	1.146	$v_{\rm st} + v_{\rm inv}$
$A_g$	332.64	3.742	0.256	38.945	10.256	157.672	3.495	$2v_{\rm b}$

ground state,  $\langle \beta_A \rangle = 27.942^\circ$  and  $\langle \beta_B \rangle = 170.13^\circ$ . This implies that the HCN molecular axis is closely aligned, to within  $10^\circ$ , with the inter-monomer axis of the complex. In the microwave spectroscopic studies of the H<sub>2</sub>O–HCN complex,  $^{30,32}$  the orientation of the HCN axis relative to the inter-monomer axis was defined by the angle that is the complement of  $\beta_B$ , and is denoted as  $\theta_{\rm av}$  in Ref. 32 and  $\gamma_a$  in Ref. 30. Their experimentally determined values,  $10.16^{\circ\,32}$  and  $9.4^\circ, ^{30}$  respectively, agree remarkably well with the complement of our calculated  $\langle \beta_B \rangle$  in the ground state,  $9.87^\circ$ .

The deviation of the  $H_2O$  moiety from the planar  $C_{2v}$  geometry of the complex is described by  $\beta_A$ , the H<sub>2</sub>O out-of-plane bend angle, whose magnitude depends on the extent of the vibrational averaging. It should be noted that because of the way that this polar angle (as well as  $\beta_B$ ) is defined, and ranges from 0 to 180°, its values can only be positive. Hence, the expectation value  $\langle \beta_A \rangle$  is always nonzero and positive, even when the equilibrium geometry is planar, corresponding to  $\beta_A = 0^{\circ}$ . From Table I, the calculated ground-state value of  $\langle \beta_A \rangle$ , 27.94°, reflects the large-amplitude character of the out-of-plane bend vibration. This result compares favorably with the spectroscopic value for this angle of 20° in Ref. 30 (denoted there as  $\theta_x$ ). On the other hand, the microwave spectroscopic study in Ref. 32 reports for this angle (denoted there as  $\phi_{av}$ ) the value of 50.9°. Such an unusually large value is attributed to the vibrational averaging over the large-amplitude out-of-plane bending motion of H<sub>2</sub>O in the complex, determined from the nuclear quadrupole coupling constants.

Finally, our computed ground-state expectation value of the intermonomer distance,  $\langle r_0 \rangle = 3.776$  Å, from Table I, is in excellent agreement with the intermonomer c.m. to c.m. distance

deduced from microwave spectroscopy, 3.765 and 3.773 Å (depending on the model employed) in Ref. 32 and 3.777 Å in Ref. 30.

We conclude that the ground-state expectation values of the intermolecular coordinates from our quantum 5D calculations on the new PES agree well with the corresponding spectroscopic values that are available in the literature. This comes with the caveat that the determination of the geometric parameters of fluxional complexes directly from spectroscopic data involves a chain of simplifying assumptions and approximations of highly reduced dimensionality whose validity is questionable, making the comparison with theory far from unambiguous.

#### B. Intermolecular vibrational states

The assignment of the intermolecular vibrational states in Table I proved to be unusually difficult. The assignments are typically made in two ways. One of them is by observing how the expectation values of the appropriate intermolecular coordinates and their root-mean-square (rms) amplitudes vary from one state to another. These quantities tend to be sensitive indicators of the excitation, or lack thereof, of certain intermolecular modes. A complementary way of making the assignments is by inspecting the contour plots of the reduced probability densities (RPDs) of the eigenstates in suitably chosen internal coordinates and counting the nodal lines perpendicular to the coordinate axes. When combined, these approaches worked very well for assigning numerous excited intermolecular states of  $\rm H_2O-CO^{13}$  and  $\rm H_2O-HCl$  complex that we studied previously.

In the case of H<sub>2</sub>O-HCN, guided by the examples of H<sub>2</sub>O-CO and H2O-HCl complexes, the goal is to try to identify the fundamentals and possibly overtones of the following intermolecular vibrational modes: (1) the intermolecular stretch mode  $v_{st}$ , (2) the HCN bend mode  $v_b$  (associated with the angular coordinate  $\beta_p$ ), (3) the out-of-plane  $H_2O$  bend (or inversion) mode  $v_{inv}$  corresponding to the rotation of the H<sub>2</sub>O moiety about its a principal axis (associated with the angular coordinate  $\beta_A$ ), and (4) the H<sub>2</sub>O rock mode  $v_{\rm rock}$  corresponding to the rotation of the H<sub>2</sub>O moiety about its c principal axis. For this purpose, we inspect in Table I the coordinate expectation values  $\langle r_0 \rangle$ ,  $\langle \beta_A \rangle$  and  $\langle \beta_B \rangle$ , as well as the corresponding rms amplitudes, and observe their variations for different states. To our surprise, this approach succeeds in identifying unambiguously only the fundamental ( $v_{st}$ ) and the first overtone ( $2v_{st}$ ) of the intermolecular stretch mode, at 128.65 and 251.13 cm<sup>-1</sup>, respectively, for which  $\langle r_0 \rangle$  and  $\Delta r_0$  increase significantly with the number of quanta. Their respective values (in Å) are 3.776 and 0.109 for the ground state, 3.824 and 0.190 for  $v_{st}$ , and 3.877 and 0.248 for  $2v_{st}$ . At the same time, for these states the values of  $\langle \beta_A \rangle$  and  $\langle \beta_B \rangle$  remain similar to those for the ground state. This makes it straightforward to identify the intermolecular stretch and its excitations.

These assignments are confirmed by examining the contour plots of the reduced probability densities (RPDs) of the two intermolecular stretch states in Fig. 5. Their nodal patterns are very regular and clearly show nodes along the intermolecular coordinate  $r_0$ , one for  $v_{st}$  and two for  $2v_{st}$ .

However, the assignment of the states corresponding primarily to the excitations of the angular degrees of freedom (DOFs) of the complex turns out to be much more challenging. For example, the state at 174.29 cm<sup>-1</sup> in Table I is nominally assigned as  $v_b$  based on the value of  $\langle \beta_B \rangle$  which is considerably smaller than for the ground state. But, at the same time its  $\langle \beta_A \rangle$  is significantly larger than in the ground state, indicating simultaneous excitation of the H<sub>2</sub>O inversion mode. The same is observed for the state at 332.64 cm<sup>-1</sup> (nominally) assigned as the first overtone of the HCN bend  $2v_b$  based on further decrease in the value of  $\langle \beta_B \rangle$ . Its  $\langle \beta_A \rangle$  is even larger than

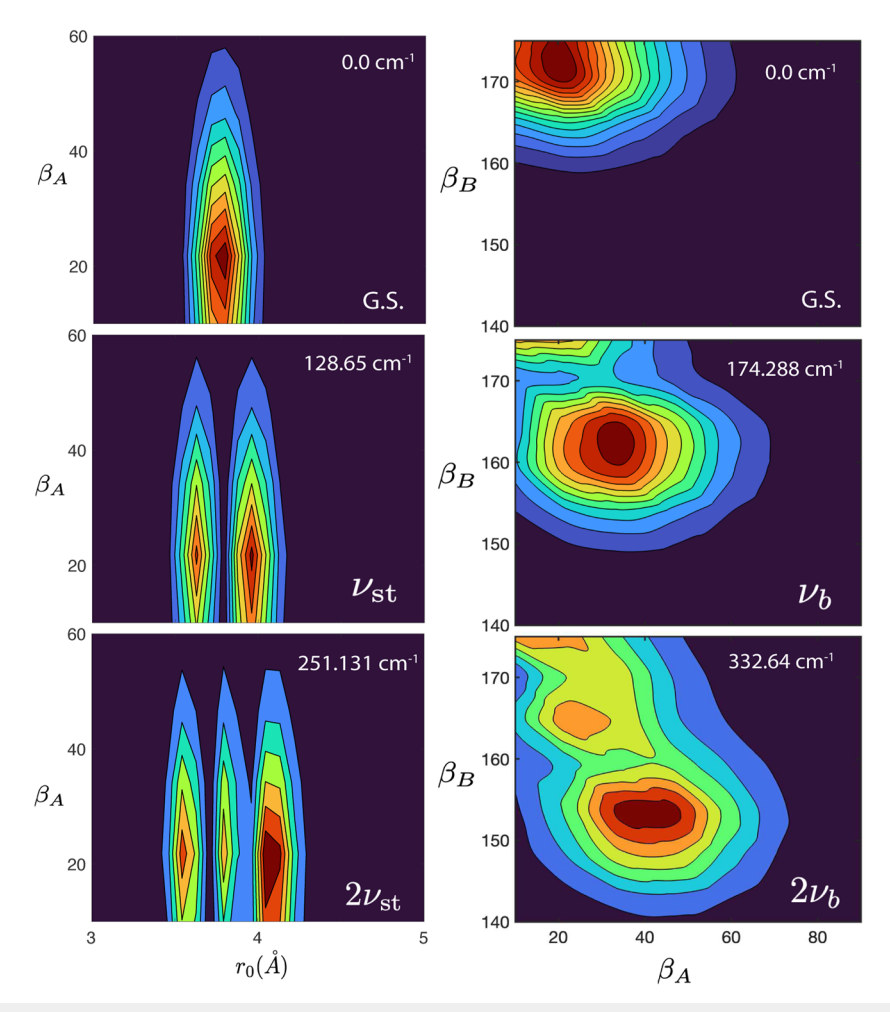


**FIG. 5.** Contour plots of the reduced probability densities, as a function of the coordinates  $r_0$  and  $\beta_A$  (in deg) (left column), and  $\beta_A$  and  $\beta_B$  (in deg) (right column), defined in the text, for the following states in Table I: the ground state of H<sub>2</sub>O–HCN (top left and right panels),  $v_{\rm st}$  (middle left),  $2v_{\rm st}$  (bottom left),  $v_{\rm b}$  (middle right), and  $2v_{\rm b}$  (bottom right).

for  $v_b$ , demonstrating again that the excitation of the HCN bend mode is linked to the excitation of the H<sub>2</sub>O inversion.

Some support for the above assignments of the  $v_b$  and  $2v_b$ states is lent by the contour plots of their RPDs in Fig. 5. They do exhibit one and two nodes, respectively, along  $\beta_B$ , and none on the

The above shows that the HCN bend and H2O inversion modes, associated with the coordinates  $\beta_B$  and  $\beta_A$ , are strongly coupled. This is also evident from the small difference of only 4 cm<sup>-1</sup> between the energies of  $v_b$  and  $v_{inv}$ , 174.29 and 178.24 cm<sup>-1</sup>, respectively. Clearly, thinking about these modes as physically distinct, involving excitations of predominantly a single coordinate, is not appropriate for this complex, and their assignments have to be taken with a great deal of caution.

The coupling between  $\beta_A$  and  $\beta_B$  is consistent with the appearance of the 2D plot of the PES in Fig. 6 as a function of  $\beta_A$  and  $\beta_B$ , for minimized values of the other three intermolecular coordinates. In addition, this 2D plot shows that the PES is rather flat in the vicinity of the global minimum, for values of  $\beta_A$  ranging from  $0^{\circ}$  to about 40°. This broad minimum explains qualitatively why the expectation value of  $\beta_A$  is around 28°.

For many states in Table I, neither the trends in the expectation values of the coordinates nor the nodal patterns of the RPDs are sufficiently clear to allow even tentative assignments. This is in sharp contrast with the H<sub>2</sub>O-HCl complex that we studied previously. 15 In that case, it was possible, with one exception, to assign all intermolecular vibrational states of the complex with energies up to 380 cm<sup>-1</sup> above the ground state. A clue as to the cause of this conspicuous difference comes from the fact that in the case of H<sub>2</sub>O-HCl none of the states in the energy range considered involves excitation of the bending mode of HCl. Evidently, this mode, being higher in energy, is only weakly coupled to the angular DOFs the H2O moiety, making the nodal patterns of the RPDs sufficiently regular for unambiguous assignment. On the other hand, in H<sub>2</sub>O-HCN, the excitations of the HCN bend mode  $v_b$  fall in the energy range of the primarily angular modes of  $H_2O$ , such as the inversion mode  $v_{inv}$ 

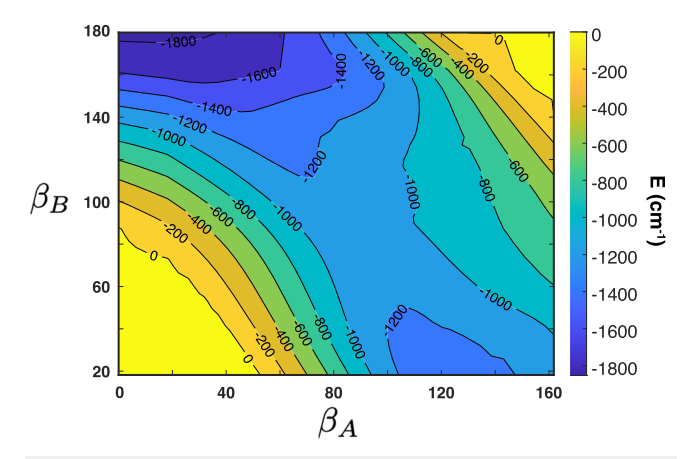


**FIG. 6.** Contour plot of the  ${\rm H_2O-HCN}$  PES as a function of  $\beta_A$  and  $\beta_B$  coordinates (in deg) (for minimized values of the three additional internal coordinates). These angles correspond to the H<sub>2</sub>O out-of-plane bend (inversion) and the HCN bend, respectively.

and the rock mode corresponding to the rotation of the H<sub>2</sub>O moiety about its c principal axis (which we could not identify). This gives rise to the strong coupling among the angular DOFs of the complex, and results in the nodal patterns of the RPDs which are too irregular for a clear-cut assignment. We believe that this difference is at least in part due to the fact that the rotational constant  $B_0$  of HCl, 10.44 cm<sup>-1</sup>, is much larger that the  $B_0$  of HCN, 1.48 cm<sup>-1</sup>.

While the coupling among the angular DOFs of the complex is strong, the radial-angular coupling, that between the intermolecular stretch and the bending modes of H<sub>2</sub>O and HCN, is apparently weak. This is evident from the remarkably regular nodal patterns of the RPDs of  $v_{st}$  and  $2v_{st}$  shown in Fig. 5, which lie among numerous, mostly unassigned, states corresponding to the excitations of the angular DOFs of the complex. Additional evidence for weak radialangular coupling comes from the fact that the expectation value of the intermonomer distance  $\langle r_0 \rangle$  changes little in the states with the excitation of the angular modes such as  $v_b$  and  $v_{inv}$ , and for any other state shown in Table I (apart from, of course,  $v_{st}$  and  $2v_{st}$ ).

Unfortunately, no spectroscopic data are available in the literature regarding the excited intermolecular vibrational states of the H<sub>2</sub>O-HCN complex that would allow comparison with the theoretical results.

As mentioned in Sec. II B, the H<sub>2</sub>O-HCN PES has two minima shown in Fig. 2, separated by a barrier of 661.84 cm<sup>-1</sup>. Given the ZPE of 364.64 cm<sup>-1</sup>, the highest-lying states in Table I with excitation energies of 290-330 cm<sup>-1</sup> have total energies of ~650-700 cm<sup>-1</sup>, that are at or slightly higher than the barrier height. Consequently, in principle, some highly excited intermolecular vibrational states of the complex could have appreciable amplitude also in the local minimum. The coordinate that is most indicative about the extent of the delocalization between two minima is  $\beta_B$ , the Euler angle between the HCN principal axis and the intermonomer vector  $r_0$ . As already discussed in Sec. IV A, when  $\beta_B = 180^{\circ}$ , the H atom of HCN is the one closest to the c.m. of H<sub>2</sub>O, corresponding to the H<sub>2</sub>O···HCN isomer/global minimum. On the other hand, when  $\beta_R = 0^{\circ}$ , it is the N atom of HCN that is the closest to the c.m of the H<sub>2</sub>O moiety, corresponding to the HCN···H<sub>2</sub>O isomer/local minimum. It is therefore reasonable to choose  $\beta_B = 90^{\circ}$  as the dividing angle between the two isomer basins on the PES. The states for which  $\langle \beta_B \rangle$ , the expectation value of  $\beta_B$ , is greater than 90° are taken to be localized is the global minimum, while those for which  $\langle \beta_{\rm R} \rangle < 90^{\circ}$  are substantially delocalized over the local minimum as well. This provides a simple numerical criterion for the quick identification of highly delocalized states. It is possible to go one step further and actually calculate for each state the eigenstate amplitudes on both sides of the dividing angle, as was done for H<sub>2</sub>O-CO, <sup>13</sup> but this was not necessary in this case. A glance at Table I shows that for all intermolecular vibrational states in it  $\langle \beta_R \rangle$  is always significantly larger than 90°, in fact it is never smaller than 150°. Thus, all these states are fully localized within the basin of the H<sub>2</sub>O···HCN global minimum, without any amplitude in the HCN···H<sub>2</sub>O local minimum. The  $2v_b$  state in Table I, for which  $\langle \beta_p \rangle$  is the smallest, 157.67°, has the RPD that extends the furthest towards the local minimum, as shown in the bottom right panel of Fig. 5. However, a comparison of this RPD with the 2D plot of the PES in the same coordinates shows clearly that it is entirely localized within the basin of the global minimum, confirming the conclusion based on the value of  $\langle \beta_R \rangle$ .

#### C. J = 1 intermolecular rovibrational states

Selected low-energy J = 1, K = 0 and J = 1, K = 1 intermolecular rovibrational states are presented in Table II. Their energies are relative to that of the J = 1 ground state energy of the dimer at -1488.138 cm<sup>-1</sup>, which is 0.2 cm<sup>-1</sup> above the J = 0 ground state. The states that are assigned to the fundamentals of the intermolecular stretch, HCN bend, and H<sub>2</sub>O inversion modes, respectively, are those that are unambiguously related to their J = 0 counterparts in Table I. It is evident that the K = 1 intermolecular states are closely spaced doublets (to within a tiny fraction of a wavenumber) and, strictly speaking, the label K stands for the absolute value |K|. Comparison of the J = 1, K = 0 states with the corresponding J = 0 states in Table I shows that they differ in energy by at most 0.002 cm<sup>-1</sup>. For several intermolecular states shown in Table II, K = 0 state is calculated to lie above K = 1 state. This is not without a precedent among weakly bound complexes. Such anomalous ordering of K = 0 and K = 1 levels has been observed previously in the calculations, and also spectroscopically, for the weakly bound water-CO complex.5,13

Inspection of Table II reveals significant variations of the  $E_{J=1,|K|=1}-E_{J=1,K=0}$  energy differences for the intermolecular states shown there. Thus,  $E_{J=1,|K|=1}-E_{J=1,K=0}$  is equal to 14.39 cm<sup>-1</sup> for the ground intermolecular state, 14.29 cm<sup>-1</sup> for the intermolecular stretch fundamental  $v_{\rm st}$ , 5.83 cm<sup>-1</sup> for the HCN bend fundamental  $v_{\rm b}$ , and 9.67 cm<sup>-1</sup> for the H<sub>2</sub>O inversion fundamental  $v_{\rm inv}$ . The largest  $E_{J=1,|K|=1}-E_{J=1,K=0}$  energy difference of 31.81 cm<sup>-1</sup> is exhibited by the unassigned state at 112.51 cm<sup>-1</sup>. Similar variation of  $E_{J=1,|K|=1}-E_{J=1,K=0}$  energy differences was found in the

**TABLE II.** Low-energy J = 1 intermolecular rovibrational states of the  $H_2O$ -HCN complex from the quantum 5D calculations.

Intermolecular state	K	Irrep.	$\Delta E (\text{cm}^{-1})^{\text{a}}$
	0	$A_u$	0.0
	1	$\mathrm{B}_u$	14.391
	1	$B_g$	14.392
	1	$A_u$	91.098
g.s.	1	$A_g$	91.099
	0	$\mathbf{B}_{u}$	94.631
	0	$\mathrm{B}_{g}$	112.514
	1	$A_g$	144.325
	1	$A_u$	144.325
	0	$A_u$	128.646
$ u_{ m st}$	1	$\mathrm{B}_u$	142.935
	1	$B_g$	142.936
	0	$A_u$	174.288
$ u_{ m b}$	1	$\mathrm{B}_u$	180.118
	1	$B_g$	180.121
	0	$\mathbf{B}_{g}$	178.238
	1	$A_g$	187.910
41	1	$A_u$	187.910
$ u_{ m inv}$	1	$A_u$	214.694
	1	$A_g$	214.695
	0	$B_u$	217.664

 $<sup>^{</sup>a}\Delta E$  is a state's energy relative to that of the J=1 ground state of the dimer.

full-dimensional rovibrational calculations of HCl-H2O/DCl-H2O complexes,<sup>17</sup> in particular the small change relative to the groundstate value upon the excitation of the  $v_{st}$  and a significant decrease accompanying the excitation of the  $v_{\text{inv}}$  mode. In fact,  $E_{J=1,|K|=1}$  $-E_{I=1,K=0}$  energy differences calculated for the ground state,  $v_{st}$ , and  $v_{\rm inv}$  modes are similar (to within less than 1 cm<sup>-1</sup>) for H<sub>2</sub>O-HCN and HCl-H<sub>2</sub>O/DCl-H<sub>2</sub>O<sup>17</sup> complexes. In Ref. 17, these variations were explained qualitatively by considering how the excitations of various intermolecular modes affect the vibrationally averaged positions of the H atoms of H<sub>2</sub>O, which in turn change the magnitude of the A rotational constant of the complex and thus the difference  $E_{J=1,|K|=1} - E_{J=1,K=0}$ . It is expected that similar arguments apply to  $H_2O-HCN$  as well, i.e., that the variations of  $E_{I=1,|K|=1}$  $-E_{J=1,K=0}$  correlate with the extent of the deviation of the vibrationally averaged geometry of the complex, caused by the excitation of an intermolecular vibrational mode, from that of the ground state.

# D. Rotational constants and rotational transition frequencies

The calculated low-energy J=1 and J=2 rotational states of the H<sub>2</sub>O–HCN complex in the ground intermolecular vibrational state from the quantum 5D calculations are given in Table III. They are measured from their quantum 5D ground-state energy at  $-1488.342~{\rm cm}^{-1}$ . H<sub>2</sub>O–HCN is an asymmetric top and its rotational levels are labeled as  $J_{K_aK_c}$ , where J is the total angular momentum and  $K_a$  and  $K_c$  are its projections on the a and c principal axes, respectively. The energies of these rotational levels are used to calculate the rotational transition frequencies for the H<sub>2</sub>O–HCN complex listed in Table IV. Also given for comparison there are the experimental values by Fillery-Travis  $et~al.^{31}$  A comparison of the computed and measured rotational transition frequencies reveals their very good agreement. For the transitions shown, the theory and experiment differ by about 20 MHz (10 MHz for the  $1_{01}$ – $0_{00}$  transition), or 0.16%.

Table V gives the ground-state rotational constants A, B, and C of  $H_2O$ –HCN based on the 5D rigid-monomer calculations of the J=1 intermolecular rovibrational states, as outlined in Sec. III B 4. The calculated B and C rotational constants are compared with the corresponding experimental values from Ref. 31. It is easy to see that the agreement is excellent, the two sets of values differing by no

**TABLE III.** Rotational states in the vibrational ground state of  $\rm H_2O-HCN$  from the quantum 5D calculations.

Assign.	$\Delta E  (\mathrm{cm}^{-1})$	Irrep.	
000	0	$A_g$	
101	0.2031	$A_u$	
111	14.5942	$B_u$	
110	14.5951	$\mathrm{B}_g$	
$2_{02}$	0.6093	$A_g$	
$2_{12}$	14.9994	$B_g$	
211	15.0020	$B_u$	
2 <sub>21</sub>	58.1026	$A_u$	
2 <sub>20</sub>	58.1026	$A_g$	

TABLE IV. Calculated and observed rotational transition frequencies (in MHz) in the vibrational ground state of H<sub>2</sub>O-HCN. The observed values are from Ref. 31.

Transition	Observed	Calculated	
1 <sub>01</sub> -0 <sub>00</sub>	6 098.8132(9)	6 088.7848	
$2_{12}-1_{11}$	12 168.0234(21)	12 147.5903	
$2_{02}-1_{01}$	12 197.4643(6)	12 177.5697	
$2_{11} - 1_{10}$	12 219.2567(36)	12 198.5551	

TABLE V. Calculated and experimentally derived rotational constants (in GHz) of the H<sub>2</sub>O-HCN complex in the ground vibrational state. The measured values are from

	Calculated	Measured
$\overline{A}$	434.492	
В	3.057	3.062
C	3.032	3.036
(B+C) (B-C)	6.089	6.099
(B-C)	0.025	0.025

more than 0.16%. Since the rotational constants B and C have similar values, the H<sub>2</sub>O-HCN complex can be viewed as near-prolate symmetric top.

These results, together with those for the rotational transition frequencies in Table IV, show that the PES employed describes with high accuracy the rotational properties of the H<sub>2</sub>O-HCN complex in the ground vibrational state.

#### V. CONCLUSIONS

In this work, the H<sub>2</sub>O-HCN system has been comprehensively characterized in two ways. First, we present a new rigid-monomer 5D intermolecular PES for the H<sub>2</sub>O-HCN complex, calculated using the SAPT(DFT) method. The calculations were conducted for 2833 ab initio points employing the aug-cc-pVQZ basis set, utilizing the autoPES code, which provides a site-site analytical fit with longrange given by perturbation theory. Our results demonstrate a level of accuracy comparable to those obtained through the CCSD(T) method with the CBS basis set. The methodology used for the PES calculations in this study can be extended to other systems interacting with water, which holds significant relevance for scattering calculations in astrophysical applications.

The newly developed PES is utilized in this paper in the quantum 5D calculations of the fully coupled intermolecular rovibrational states of the H<sub>2</sub>O-HCN complex in the rigid-monomer approximation for the total angular momentum J values of 0, 1, and 2. These calculations rely on the methodology employed previously in the quantum 5D rigid-monomer calculations of the rovibrational states of the H<sub>2</sub>O-CO<sub>2</sub> and D<sub>2</sub>O-CO<sub>2</sub> vdW complexes,<sup>1</sup> and also utilized in all our recent full-dimensional (9D) quantum calculations of the (ro)vibrational states of noncovalently bound triatom-diatom complexes. 12-16 Whenever possible, our theoretical results are compared with the spectroscopic data in the literature. The ground-state expectation values of the intermolecular coordinates of the complex (the intermonomer distance, the angle between the HCN molecular axis and the intermonomer axis, the H2O outof-plane bend angle) from our quantum 5D calculations on the new PES agree very well with the available microwave spectroscopy measurements. In addition, the computed ground-state rotational transition frequencies involving the J = 0, 1 and 2 rotational states of H<sub>2</sub>O-HCN, as well as the B and C rotational constants calculated for the ground state of the complex, are in excellent agreement, to within 0.16%, with the experimental values. From this, one can conclude that the new PES describes with high accuracy the rotational properties of the H<sub>2</sub>O-HCN complex in the ground vibrational states.

Highly converged intermolecular vibrational states of H<sub>2</sub>O-HCN from the quantum 5D calculations are reported for energies up to about 350 cm<sup>-1</sup> above the ground state of the complex. Their assignment proved to be surprisingly challenging. Only the fundamental and the first overtone of the intermolecular stretch mode can be identified unambiguously. Due to the unusually strong coupling among the angular degrees of freedom of the complex, most of the other excited states remain unassigned. One explanation for the strong angular coupling involves the small rotational constant  $B_0$  of HCN (1.48 cm<sup>-1</sup>), as a result of which the excitations of the HCN bend mode fall in the energy range of the angular modes of H2O moiety and strongly couple with them. In contrast, the radial-angular coupling, between the intermolecular stretch and the bending modes of the two monomers, is evidently weak, allowing straightforward assignment of its excitations.

We hope that the calculations reported in this paper will motivate spectroscopic investigations of the excited intermolecular vibrational states of the H<sub>2</sub>O-HCN, which would allow a more detailed assessment of the accuracy of the new PES and guide its improvements.

#### SUPPLEMENTARY MATERIAL

The computer code for generating the H<sub>2</sub>O-HCN PES reported in this work is provided, together with the Readme.txt file with the information on how to execute it.

#### **ACKNOWLEDGMENTS**

Z.B, P.M.F., and P.V.Z. are grateful to the National Science Foundation for its partial support of this research through the Grant Nos. CHE-2054616 and CHE-2054604. They are also grateful to the Simons Foundation for the computational resources acquired with its support, that were used in this research. P.M.F. is grateful to Professor Daniel Neuhauser for his support. J.K. is grateful to the US National Science Foundation for support through Grant No. AST-2009253 (Subaward No. 362627Sub1). D.K. and P.S.Z. are grateful to the National Science Centre (NCN) for funding the project Sonata Bis 9 2019/34/E/ST4/00407 and the COST Action CA21101 Confined Molecular Systems: From a New Generation of Materials to the Stars (COSY). F.L. and M.Z. acknowledge financial support from the European Research Council (Consolidator Grant COLLEXISM, Grant Agreement No. 81163). F.L. acknowledges the Institut Universitaire de France and Rennes Metropole for the financial support.

#### **AUTHOR DECLARATIONS**

#### **Conflict of Interest**

The authors have no conflicts to disclose.

#### **Author Contributions**

Patricia Vindel-Zandbergen: Conceptualization (equal); Formal analysis (equal); Funding acquisition (equal); Methodology (equal); Visualization (equal); Writing - original draft (equal); Writing review & editing (equal). Dariusz Kędziera: Conceptualization (equal); Formal analysis (equal); Funding acquisition (equal); Methodology (equal); Writing - original draft (equal); Writing review & editing (equal). Michał Żółtowski: Conceptualization (equal); Formal analysis (equal); Methodology (equal); Visualization (equal); Writing – original draft (equal); Writing – review & editing (equal). Jacek Kłos: Conceptualization (supporting); Funding acquisition (equal); Methodology (equal); Visualization (equal); Writing – original draft (equal); Writing - review & editing (equal). Piotr Żuchowski: Conceptualization (equal); Formal analysis (equal); Funding acquisition (equal); Methodology (equal); Writing - original draft (equal); Writing - review & editing (equal). Peter M. Felker: Conceptualization (equal); Formal analysis (equal); Funding acquisition (equal); Methodology (equal); Writing - original draft (equal); Writing - review & editing (equal). François Lique: Conceptualization (equal); Funding acquisition (equal); Supervision (equal); Writing - original draft (equal); Writing - review & editing (equal). Zlatko Bačić: Conceptualization (equal); Formal analysis (equal); Funding acquisition (equal); Methodology (equal); Supervision (equal); Writing - original draft (equal); Writing - review & editing (equal).

#### **DATA AVAILABILITY**

The data that support the findings of this study are available within the article and its supplementary material.

#### **REFERENCES**

- <sup>1</sup>P. M. Felker and Z. Bačić, J. Chem. Phys. **156**, 064301 (2022).
- <sup>2</sup>J. Loreau, Y. N. Kalugina, A. Faure, A. van der Avoird, and F. Lique, J. Chem. Phys. 153, 214301 (2020).
- <sup>3</sup>D. Viglaska, X.-G. Wang, T. Carrington, Jr., and D. P. Tew, J. Mol. Spectrosc. 384, 111587 (2022).
- <sup>4</sup>Y. N. Kalugina, A. Faure, A. van der Avoird, K. Walker, and F. Lique, Phys. Chem. Chem. Phys. 20, 5469 (2018).
- <sup>5</sup> A. J. Barclay, A. van der Avoird, A. R. W. McKellar, and N. Moazzen-Ahmadi, Phys. Chem. Chem. Phys. 21, 14911 (2019).
- <sup>6</sup>S. A. Ndengue, Y. Scribano, D. M. Benoit, F. Gatti, and R. Dawes, Chem. Phys. Lett. 715, 347 (2019).
- <sup>7</sup>X.-G. Wang and T. Carrington, Jr., J. Chem. Phys. **134**, 044313 (2011).
- <sup>8</sup> A. van der Avoird and D. J. Nesbitt, J. Chem. Phys. **134**, 044314 (2011).
- <sup>9</sup>X.-G. Wang and T. Carrington, J. Chem. Phys. **154**, 124112 (2021).
- <sup>10</sup> A. M. S. Daria, G. Avila, and E. Mátyus, J. Chem. Phys. **154**, 224302 (2021).
- <sup>11</sup>P. M. Felker and Z. Bačić, J. Chem. Phys. **151**, 024305 (2019).
- <sup>12</sup>P. M. Felker and Z. Bačić, Phys. Chem. Chem. Phys. **24**, 24655 (2022).
- <sup>13</sup>P. M. Felker and Z. Bačić, J. Chem. Phys. **153**, 074107 (2020).
- <sup>14</sup>P. M. Felker and Z. Bačić, J. Phys. Chem. A 125, 980 (2021).
- <sup>15</sup>Y. Liu, J. Li, P. M. Felker, and Z. Bačić, Phys. Chem. Chem. Phys. 23, 7101 (2021).

- <sup>16</sup>P. M. Felker, Y. Liu, J. Li, and Z. Bačić, J. Phys. Chem. A **125**, 6437 (2021).
- <sup>17</sup>P. M. Felker and Z. Bačić, Chin. J. Chem. Phys. 34, 728 (2021).
- <sup>18</sup>P. M. Felker and Z. Bačić, J. Chem. Phys. **152**, 124103 (2020).
- <sup>19</sup> X.-G. Wang and T. Carrington, J. Chem. Phys. **158**, 084107 (2023).
- <sup>20</sup> M. A. Cordiner, N. X. Roth, S. N. Milam, G. L. Villanueva, D. Bockelée-Morvan, A. J. Remijan, S. B. Charnley, N. Biver, D. C. Lis, C. Qi, B. P. Bonev, J. Crovisier, and J. Boissier, Astrophys. J. 953(1), 59 (2023).
- <sup>21</sup> N. Biver, D. Bockelée-Morvan, J. Crovisier, Aa. Sandqvist, J. Boissier, D. C. Lis, M. Cordiner, B. P. Bonev, N. Dello Russo, R. Moreno, S. Milam, N. X. Roth, R. Vervack, and M. A. DiSanti, Astron. Astrophys. 672, A170 (2023).
- <sup>22</sup>A. Hinchliffe, J. Mol. Struct.: THEOCHEM **136**, 193–199 (1986).
- <sup>23</sup> A. C. Samuels, J. O. Jensen, P. N. Krishnan, and L. A. Burke, J. Mol. Struct.: THEOCHEM 427(1-3), 199-209 (1998).
- <sup>24</sup>R. Rivelino and S. Canuto, Chem. Phys. Lett. **322**, 207 (2000).

Chem. A 103, 2945 (1999).

- <sup>25</sup>R. Rivelino and S. Canuto, J. Phys. Chem. A **105**, 11260 (2001).
- <sup>26</sup>T. Malaspina, E. E. Fileti, J. M. Riveros, and S. Canuto, J. Phys. Chem. A 110, 10303 (2006).
- E. Q. Sánchez and M. L. Dubernet, Phys. Chem. Chem. Phys. 19, 6849 (2017).
   A. Heikkilä, M. Pettersson, J. Lundell, L. Khriachtchev, and M. Räsänen, J. Phys.
- <sup>29</sup> M. L. Dubernet and E. Quintas-Sánchez, Mol. Astrophys. 16, 100046 (2019).
- <sup>50</sup> H. S. Gutowsky, T. C. Germann, J. D. Augspurger, and C. E. Dykstra, J. Chem. Phys. **96**, 5808 (1992).
- <sup>31</sup> A. J. Fillery-Travis, A. C. Legon, and L. C. Willoughby, Chem. Phys. Lett. 98, 369 (1983).
- $^{\bf 32}$  A. J. Fillery-Travis, A. C. Legon, and L. C. Willoughby, Proc. R. Soc. London, Ser. A  $\bf 396, 405 \ (1984).$
- <sup>33</sup> A. J. Misquitta, R. Podeszwa, B. Jeziorski, and K. Szalewicz, J. Chem. Phys. 123, 214103 (2005).
- <sup>34</sup> M. P. Metz and K. Szalewicz, J. Chem. Phys. **152**, 134111 (2020).
- <sup>35</sup> M. P. Metz, K. Piszczatowski, and K. Szalewicz, J. Chem. Theory Comput. 12, 5895 (2016).
- <sup>36</sup> A. J. Misquitta, B. Jeziorski, and K. Szalewicz, Phys. Rev. Lett. **91**, 033201 (2003).
- <sup>37</sup> A. Heßelmann, G. Jansen, and M. Schütz, J. Chem. Phys. **122**, 014103 (2004).
- <sup>38</sup> J. Garcia, R. Podeszwa, and K. Szalewicz, J. Chem. Phys. **152**, 184109 (2020).
- <sup>39</sup> D. E. Taylor, J. G. Ángyán, G. Galli, C. Zhang, F. Gygi, K. Hirao, J. W. Song, K. Rahul, O. Anatole von Lilienfeld, R. Podeszwa, I. W. Bulik, T. M. Henderson, G. E. Scuseria, J. Toulouse, R. Peverati, D. G. Truhlar, and K. Szalewicz, J. Chem. Phys. 145, 124105 (2016).
- <sup>40</sup>C. Adamo and V. Barone, J. Chem. Phys. **110**(13), 6158–6170 (1999).
- <sup>41</sup>T. H. Dunning, J. Chem. Phys. **90**, 1007 (1989).
- <sup>42</sup>D. E. Woon and T. H. Dunning, J. Chem. Phys. **100**, 2975 (1994).
- <sup>43</sup>R. A. Kendall, T. H. Dunning, and R. J. Harrison, J. Chem. Phys. **96**, 6796 (1992).
- <sup>44</sup>M. Grüning, O. V. Gritsenko, S. J. A. van Gisbergen, and E. J. Baerends, J. Chem. Phys. 114, 652 (2001).
- 45 G. Czakó, E. Mátyus, and A. G. Császár, J. Phys. Chem. A 113, 11665 (2009).
- <sup>46</sup>I. M. Mills, J. Phys. Chem. **80**, 1187 (1976).
- 47 M. Iliaš and T. Saue, J. Chem. Phys. 126, 064102 (2007).
   48 W. Gisbert, G. M. Arthur, and G. Winnewisser, J. Mol. Spectrosc. 39, 149 (1971).
- <sup>49</sup>CFOUR, a quantum chemical program package, J. F. Stanton, J. Gauss, L. Cheng, M. E. Harding, D. A. Matthews, P. G. Szalay with contributions from A. A. Auer, R. J. Bartlett, U. Benedikt, C. Berger, D. E. Bernholdt, Y. J. Bomble, O. Christiansen, F. Engel, R. Faber, M. Heckert, O. Heun, C. Huber, T.-C. Jagau, D. Jonsson, J. Jusélius, K. Klein, W. J. Lauderdale, F. Lipparini, T. Metzroth, L. A. Mück, D. P. O'Neill, D. R. Price, E. Prochnow, C. Puzzarini, K. Ruud, F. Schifmann, W. Schwalbach, C. Simmons, S. Stopkowicz, A. Tajti, J. Vázquez, F. Wang, J. D. Watts and the integral packages MOLECULE (J. Almlöf and P. R. Taylor), PROPS (P. R. Taylor), ABACUS (T. Helgaker, H. J. A. Jensen, P. Jørgensen, and
- <sup>50</sup>CFOUR, A Quantum Chemical Program Package.

version, see https://cfour.uni-mainz.de/cfour/.

<sup>51</sup>T. R. Phillips, S. Maluendes, A. D. McLean, and S. Green, J. Chem. Phys. **101**, 5824 (1994).

J. Olsen), and ECP routines by A. V. Mitin and C. van Wüllen, For the current

<sup>52</sup>H.-J. Werner, P. J. Knowles, G. Knizia, F. R. Manby, M. Schütz, P. Celani, W. Györffy, D. Kats, T. Korona, R. Lindh, A. Mitrushenkov, G. Rauhut, K. R. Shamasundar, T. B. Adler, R. D. Amos, S. J. Bennie, A. Bernhardsson, A. Berning, D. L. Cooper, M. J. O. Deegan, A. J. Dobbyn, F. Eckert, E. Goll, C. Hampel, A. Hesselmann, G. Hetzer, T. Hrenar, G. Jansen, C. Köppl, S. J. R. Lee, Y. Liu, A. W. Lloyd, Q. Ma, R. A. Mata, A. J. May, S. J. McNicholas, W. Meyer, T. F. Miller III, M. E. Mura, A. Nicklass, D. P. O'Neill, P. Palmieri, D. Peng, K. Pflüger, R. Pitzer, M. Reiher, T. Shiozaki, H. Stoll, A. J. Stone, R. Tarroni, T. Thorsteinsson, M. Wang, and M. Welborn, MOLPRO, version 2019.2, a package of *ab initio* programs, 2019, https://www.molpro.net.

<sup>53</sup> K. A. Peterson, D. E. Woon, and T. H. Dunning, J. Chem. Phys. **100**, 7410 (1994).

- <sup>54</sup>G. Brocks, A. van der Avoird, B. T. Sutcliffe, and J. Tennyson, Mol. Phys. 50, 1025 (1983).
- <sup>55</sup>E. B. Wilson, J. C. Decius, and P. C. Cross, Molecular Vibrations; the Theory of infrared and Raman Vibrational Spectra (McGraw-Hill, New York, 1955).
- <sup>56</sup>J. Echave and D. C. Clary, Chem. Phys. Lett. **190**, 225 (1992).
- <sup>57</sup> H. Wei and T. Carrington, Jr., J. Chem. Phys. **97**, 3029 (1992).
- <sup>58</sup>V. A. Mandelshtam and H. S. Taylor, J. Chem. Phys. **106**, 5085 (1997).
- <sup>59</sup>G. Herzberg, Molecular Spectra and Molecular Structure II. Infrared and Raman Spectra of Polyatomic Molecules (Van Nostrand, Princeton, 1966).